



Bloch-type domain walls in rhombohedral BaTiO₃

Maryam Taherinejad* and David Vanderbilt

Department of Physics and Astronomy, Rutgers University, Piscataway, New Jersey 08854-0849, USA

Pavel Marton, Vilgelmina Stepkova, and Jiri Hlinka

Institute of Physics, Academy of Sciences of the Czech Republic, Na Slovance 2, 18221 Praha 8, Czech Republic

(Received 20 August 2012; published 22 October 2012)

Ferroelectric domain walls (FDWs) are usually considered to be of Ising type, but there have been suggestions in recent years that Bloch-type FDWs are also possible in some cases, e.g., in the rhombohedral phase of BaTiO₃. The mechanically compatible and electrically neutral FDWs in rhombohedral BaTiO₃ are of 71°, 109°, and 180° type. We have investigated these FDWs based both on first-principles calculations and on a Ginzburg-Landau-Devonshire (GLD) model [P. Marton, I. Rychetsky, and J. Hlinka, *Phys. Rev. B* **81**, 144125 (2010)]. The results from both approaches confirm the Ising nature of the 71° FDW and the Bloch nature of the 180° FDW, and predict both Ising-type and Bloch-type FDWs are possible for the 109° case. Considering the relatively small rhombohedral strain in BaTiO₃, the competition between the energies of Bloch and Ising FDWs can be discussed in terms of a picture in which a Bloch wall is regarded as being composed of a pair of smaller-angle Ising ones. A reduction by 40% in the parameters describing the gradient term in the GLD model brings it into better agreement with the first-principles results for detailed properties such as the energies and widths of the FDWs.

DOI: [10.1103/PhysRevB.86.155138](https://doi.org/10.1103/PhysRevB.86.155138)

PACS number(s): 77.80.Dj, 77.22.Ej, 77.84.—s

I. INTRODUCTION

Ferroelectrics find many industrial and commercial applications, such as in high-dielectric constant capacitors, ferroelectric thin-film memories, piezoelectric transducers, nonlinear optical devices, and switches. The performance of many kinds of ferroelectric devices is affected by the ferroelectric domain structure and the properties of the domain boundaries. For example, a recent experiment has shown that the observed dielectric permittivity of a BaTiO₃ single crystal in the rhombohedral phase varies depending on the domain structures induced by pretreatments at higher temperatures.¹ Such influences on the mechanical and electrical properties of devices has motivated theoretical and experimental work directed toward obtaining a better understanding of ferroelectric domain structures.

Ferroelectric domain walls (FDWs) are usually considered to be of Ising type, in which \mathbf{P}_{\parallel} , the projection of the polarization vector onto the plane of the domain wall, simply reverses itself by passing through zero along a high-symmetry path as one scans through the domain wall. Ising FDWs tend to be favored because ferroelectrics are generally strongly electrostrictive, so that a rotation of \mathbf{P}_{\parallel} away from this high-symmetry path would entail a significant elastic energy cost. In contrast, the spontaneous magnetostriction which couples the magnetization and lattice strain in ferromagnetic materials is typically much weaker. As a result, magnetic domain walls are usually much wider, on the order of microns, and the magnetization vector can rotate away from the high-symmetry path. The domain wall is denoted as a Bloch or Néel wall depending on whether this rotation occurs in a plane parallel or normal to the domain wall, respectively.

In recent years, however, there have been some theoretical predictions of the presence of Bloch and even Néel components in some ferroelectric materials and heterostructures.^{2–4} In particular, it has been predicted, in the framework of a

phenomenological Ginzburg-Landau-Devonshire (GLD) model, that the 180° FDWs in rhombohedral BaTiO₃ should be of Bloch type.⁵ This work has motivated us to test whether this behavior is also reproduced by first-principles density-functional calculations on BaTiO₃.

Since the discovery of ferroelectricity in this material in 1945,^{6–8} BaTiO₃ has been very widely studied and has emerged as a kind of prototypical ferroelectric compound. It undergoes a sequence of phase transitions from a high-temperature paraelectric cubic phase to ferroelectric tetragonal, orthorhombic, and finally rhombohedral phases as the temperature is reduced. Here, we are interested in the zero-temperature rhombohedral phase, in which the spontaneous polarization prefers to lie in eight energetically equivalent directions, as shown by the arrows in Fig. 1. The figure also shows the possible rotation angles between the spontaneous polarization directions on the two sides of the domain wall (relative to the arrow marked as “0”). In the low-temperature rhombohedral phase of BaTiO₃, the FDWs are therefore of three types: R71°, R109°, and R180°. (The “R” denotes a FDW in the rhombohedral phase, following the notation of Ref. 5.) Taking into account the constraints of electrical neutrality and mechanical compatibility, the plane of the FDW is normal to the sum of the two polarization vectors for the R71° and R109° cases, while for the 180° case it can be either $\{\bar{2}11\}$ or $\{1\bar{1}0\}$.

In this work, the R71°, R109°, and R180° $\{1\bar{1}0\}$ FDWs in BaTiO₃ are investigated using first-principles calculations in the context of density-functional theory. While first-principles calculations have been successfully applied to study FDWs in many other cases,^{2,4,9,10} we are not aware of any previous application to the case of the rhombohedral phase of BaTiO₃. Our calculations confirm the Bloch nature of the R180° $\{1\bar{1}0\}$ FDW and the Ising nature of the R71° FDW, in agreement with the predictions of the GLD model. The energy difference between the Bloch R109° and Ising R109° FDW is very small,

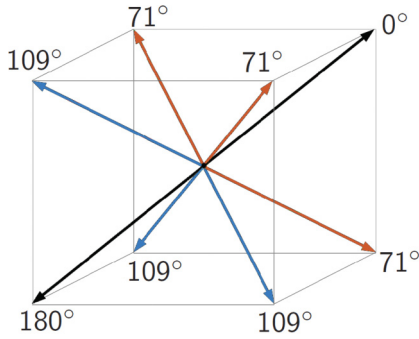


FIG. 1. (Color online) The directions of the symmetry-allowed spontaneous polarizations in rhombohedral BaTiO₃. Angles are relative to the reference direction labeled as 0°.

which suggests that both types of the domain wall are possible. The Bloch walls can be regarded as being composed of two Ising walls of smaller angles. A comparison of the sum of the energies of these constituting Ising walls with that of an Ising-type solution can explain why the polarization vector picks a Bloch-type path in some FDWs. A quantitative comparison of our first-principles results with those of the GLD model suggests that a 40% reduction in the size of a gradient term in the GLD model is needed to bring the two theories into good agreement.

The manuscript is organized as follows. In Sec. III, we describe the geometry of each of the FDWs to be studied. We also review the first-principles and GLD model approaches which are used to study the FDWs, and give the details of the methods used for the first-principles calculations. The results from the first-principles calculations and their comparison to the GLD model are then described in Sec. IV. In Sec. V, we discuss the competition between Ising and Bloch configurations in terms of energy considerations, and in Sec. VI we briefly summarize and discuss future prospects.

II. DOMAIN WALL AND SUPERCELL GEOMETRIES

The mechanically compatible and electrically neutral FDWs investigated in this paper are shown in the left column of Fig. 2, where the arrows indicate the orientation of the polarization vectors $\mathbf{P}(-\infty)$ and $\mathbf{P}(\infty)$ on the two sides of the domain wall. In the right column, the symmetry-adapted coordinate system (r, s, t) is shown for each of these walls. The unit vector normal to the wall is denoted by \mathbf{s} . The second unit vector \mathbf{r} is chosen to be parallel to $\mathbf{P}(\infty) - \mathbf{P}(-\infty)$, the difference between the spontaneous polarizations on the two sides of the wall; electrically neutrality implies that this is normal to \mathbf{s} . The third basis vector is defined as $\mathbf{t} = \mathbf{r} \times \mathbf{s}$.

For the application of the GLD continuum approach, atomistic details are not important, and specific atomistic geometries do not have to be considered. This is obviously not the case, however, for the first-principles calculations. These are set up by considering a supercell that is extended along the direction \mathbf{s} normal to the wall, keeping minimal dimensions in the orthogonal directions. Ideally, we would prefer a supercell containing only a single domain wall, but this is incompatible with periodic boundary conditions. Thus, we use supercells containing two equivalent FDWs,

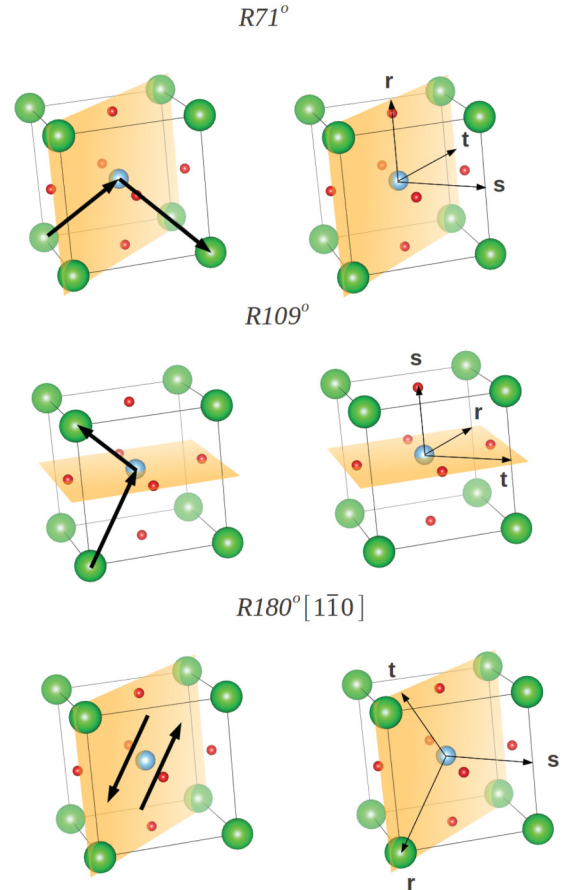


FIG. 2. (Color online) The $R71^\circ$, $R109^\circ$, and $R180^\circ\{1\bar{1}0\}$ FDWs in BaTiO₃. The arrows in the figures at left show the directions of the polarization vectors on the two sides of the domain wall, while those on the right depict the associated symmetry-adapted coordinate system (r, s, t) .

where we enforce this equivalence by imposing a twofold screw symmetry (twofold rotation about \mathbf{s} followed by a half superlattice-vector translation along the stacking direction \mathbf{s}). If these walls are well separated, their effect on each other should be small and the physical properties of the walls should be unaffected.

We first construct a reference paraelectric supercell by identifying a minimal building block having lattice vectors parallel to \mathbf{r} , \mathbf{s} , and \mathbf{t} , and repeating this block N times along the stacking direction \mathbf{s} . An example of such a building block, used for the $R71^\circ$ and $R180^\circ\{1\bar{1}0\}$ cases, is shown in Fig. 3,

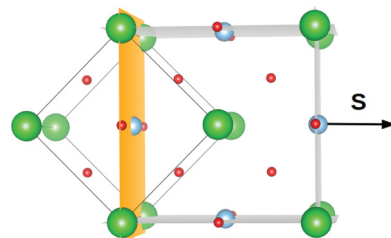


FIG. 3. (Color online) 10-atom rotated building block that is stacked along \mathbf{s} to construct supercells for studying $R71^\circ$ and $R180^\circ\{1\bar{1}0\}$ FDWs, which lie normal to \mathbf{s} .

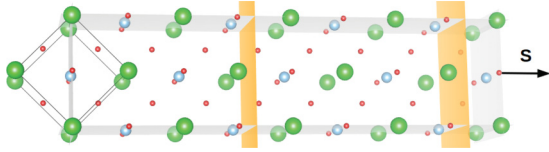


FIG. 4. (Color online) A supercell with four rotated 10-atom units stacked in the s direction. The centers of the FDWs are shown by the orange planes.

and an example of a supercell built from it is shown in Fig. 4. An initial configuration for an Ising FDW is then chosen by shifting the coordinates of the oxygen atoms along the $\mathbf{P}(-\infty)$ direction in the first half of the supercell, and along $\mathbf{P}(\infty)$ in the second half. For the $R71^\circ$ and $R109^\circ$ cases, this results in a configuration with a mirror symmetry relating the $-\mathbf{t}$ and \mathbf{t} directions, and since this symmetry is preserved by the subsequent relaxation of atomic coordinates, the resulting relaxed configuration is guaranteed to be of Ising type. To initialize a calculation on a Bloch FDW, we also add oxygen displacement components along \mathbf{t} in one FDW and along $-\mathbf{t}$ in the other (still preserving the screw symmetry), so that effectively the displacement vector in the \mathbf{r} - \mathbf{t} plane is rotated from the \mathbf{r} to the \mathbf{t} direction across the wall before pointing to $-\mathbf{r}$ on the other side of the wall. In both the Ising and Bloch cases, the s component is left unchanged in the initial configuration, although of course it may relax later.

We then relax the atomic coordinates until all of the forces fall below a chosen threshold. While doing this, we constrain the two in-plane lattice vectors (i.e., in the plane of the FDW) to remain fixed, consistent with the relaxed strain state of a single-domain rhombohedral crystal. We do this because the physical system we are trying to model is an isolated FDW between very thick domains, in which case the bulk elasticity dominates over the interface and fixes the in-plane strain. We let the third (long) superlattice vector relax along with the atomic coordinates during the minimization. Finally, the polarization profile is calculated from the pattern of displacements and the calculated dynamical effective charges as described in Sec. III A.

For all the investigated FDWs, we can always find an Ising-type FDW solution if we impose an appropriate symmetry constraint. To test whether this solution is locally stable, we add small symmetry-lowering atomic displacements, and check whether it relaxes back to the Ising solution. We next try starting from a Bloch-type configuration, with substantial distortions similar to those that would be present in well-defined domains of rhombohedral phase. Again, if this structure relaxes back to the Ising one, then we conclude that no Bloch FDW was found, and the Ising solution is stable. If we find instead that the calculation converges to a Bloch-type solution, we compare its energy with that of the Ising solution (if locally stable) to determine which is the global solution.

The $R71^\circ$ wall has its normal s in the $[1\bar{1}0]$ direction, so that it lies parallel to the diagonal plane in the primitive cell as shown in Fig. 2. Therefore, we consider the building block of Fig. 3, which is a 10-atom $\sqrt{2} \times \sqrt{2} \times 1$ cell obtained by rotating by 45° around the z axis with respect to the parent cubic unit cell. In this rotated cell, the FDW lies in the (100) plane. The simulation supercell is constructed by stacking these units in the s direction, as shown in Fig. 4. The

initial coordinates for the Ising $R71^\circ$ FDW simulation are then obtained by shifting the oxygen atoms by about 0.1 \AA along $[101]$ in half the supercell, and along $[10\bar{1}]$ in the other half, in the rotated coordinate system.

The $R109^\circ$ FDW lies in the (100) plane, $s = \hat{x}$, and a supercell can easily be made by stacking the primitive 5-atom rhombohedral cells in this direction. The initial Ising configuration is then set by displacing the oxygen atoms from the equilibrium positions along the $[111]$ direction on one side of the FDW, and along the $[1\bar{1}\bar{1}]$ direction on the other side.

The $R180^\circ\{1\bar{1}0\}$ wall is again parallel to the diagonal plane in the primitive cell, as for the $R71^\circ$ domain wall. So in this case as well, a supercell is made by stacking the rotated 10-atom units shown in Fig. 3 in the s direction. The initial configuration for the $R180^\circ\{1\bar{1}0\}$ Ising FDW is obtained by shifting the oxygen atoms from their equilibrium positions along the $[011]$ direction on one side of the FDW and along the opposite direction on the other side, in the rotated coordinate system.

For the Ising $R180^\circ\{1\bar{1}0\}$ case, there is also the possibility of imposing a higher symmetry by insisting that the FDW lie exactly in a Ba-Ti-O plane, or exactly in an O-O plane, which can be accomplished by adopting an inversion center through one of the atoms lying in the FDW. This is not possible for the $R71^\circ$ and $R109^\circ$ FDWs since the presence of a global P_s component makes the “front” and “back” sides of the FDW distinguishable and rules out the presence of an inversion symmetry.

III. COMPUTATIONAL APPROACH

A. First-principles calculations

The calculations are done using the ABINIT implementation of density functional theory¹¹ within the local-density approximation (LDA) using the Perdew-Zunger exchange-correlation functional.¹² Ultrasoft pseudopotentials,¹³ in which semicore s and p states are included in the valence for Ba and Ti, were converted for use as projector augmented-wave (PAW) potentials¹⁴ using the USPP2ABINIT package. The plane-wave cutoff and the energy cutoff for the fine fast Fourier transform (FFT) grid are set to 25 Ha and 40 Ha, respectively. The tolerance on the difference of forces in successive iterations in a self-consistent-field (SCF) cycle is set to 5.0×10^{-10} hartree/Bohr, which reached twice successively, causes one SCF cycle to stop and ions to be moved. The structural optimizations are done using the Broyden-Fletcher-Goldfarb-Shanno minimization.¹⁵

The supercells employed for studying $R71^\circ$ and $R180^\circ$ FDWs are of dimensions $\sqrt{2}Na \times \sqrt{2}a \times a$, where a is the primitive lattice constant and N is the number of 10-atom units stacked in the s direction. Therefore, a $1 \times 4 \times 6$ Monkhorst-Pack¹⁶ k -mesh is chosen for simulating these domain walls. The supercell for the $R109^\circ$ FDW is made by stacking the 5-atom primitive cells in one direction, so a $1 \times 6 \times 6$ Monkhorst-Pack¹⁶ k -mesh seems a proper choice for simulating this FDW.

We also compute the dynamical effective charges¹⁷ Z^* in bulk paraelectric cubic BaTiO₃.¹⁸ The dynamical charge tensor $Z_{i\alpha\beta}^*$ of a given atom measures the dipole induced along β by a displacement of atom i along α . In many oxides including

BaTiO₃, these charges are quite different from the formal ionic charges. The Z^* tensors are computed by finite differences, i.e., by making small displacements and calculating the resulting change in Berry-phase polarization.¹⁹

These dynamical charges are then used as an ingredient in an algorithm² by which we map out the polarization profiles in FDW-containing supercells, as follows. The polarization is only changing along the stacking direction and is constant in the planes normal to this direction. So, first the contribution from each layer to the dipole moment in direction α arising from displacements of atoms j in direction β is calculated as

$$p_\alpha^{(l)} = \sum_{\beta, j \in l} Z_{j\beta, \alpha}^* u_{j\beta}, \quad (1)$$

where l is a layer index. In the supercell used for studying the R109° FDW, these are Ba-O and Ti-O-O layers, while for the R71° and R180°{110} FDWs built from the rotated 10-atom units, l refers to Ba-Ti-O and O-O layers. If we break the supercell into smaller cells centered on these layers, we can assign a local polarization to cell l by counting its own contribution and half that of each neighbor, i.e.,

$$P_\alpha^{(l)} = \frac{1}{\Omega} \left(\frac{1}{2} p_\alpha^{(l-1)} + p_\alpha^{(l)} + \frac{1}{2} p_\alpha^{(l+1)} \right), \quad (2)$$

where Ω is the volume of the cell.

B. GLD model

We review the Ginzburg-Landau-Devonshire model used in Ref. 20, which is again used here to model the FDW properties and compare with the first-principles results. The excess free energy F relative to the reference cubic paraelectric state is expressed in terms of polarization and strain fields as

$$F[\{P_i, P_{i,j}, e_{i,j}\}] = \int f(\mathbf{r}) d\mathbf{r}, \quad (3)$$

where f is the GLD free-energy density which is taken to be a function of the polarization components P_i , their spatial derivatives $P_{i,j} = \partial P_i / \partial x_j$, and strain components $e_{i,j}$. In particular, f is expressed in terms of Landau, elastic, electrostriction, and gradient terms:

$$f = f_L^{(e)}\{P_i\} + f_c\{e_{ij}\} + f_q\{P_i, e_{ij}\} + f_G\{P_{i,j}\}. \quad (4)$$

In Ref. 20, explicit forms were given for each of the terms in this expression, parameter values were estimated from the bulk single-crystal properties of BaTiO₃, and the GLD model was used to investigate domain-wall properties.

Here, we are especially concerned with the gradient or Ginzburg terms in the free-energy expansion, which take the form

$$\begin{aligned} f_G = & \frac{1}{2} G_{11} (P_{1,1}^2 + P_{2,2}^2 + P_{3,3}^2) \\ & + G_{1,2} (P_{1,1} P_{2,2} + P_{2,2} P_{3,3} + P_{1,1} P_{3,3}) \\ & + \frac{1}{2} G_{44} [(P_{1,2} + P_{2,1})^2 + (P_{2,3} + P_{3,2})^2 \\ & + (P_{3,1} + P_{1,3})^2]. \end{aligned} \quad (5)$$

As discussed in Ref. 20, considerable caution was required in extracting the G coefficients from inelastic neutron scattering experiments, and the remaining uncertainties are significant. The G tensor has an important effect on the widths and energies

of the FDWs, so that the uncertainties in the values of these coefficients are a limiting factor in determining the properties of the FDWs. The original parameters of Ref. 5 describing the gradient terms are $G_{11} = 51 \times 10^{-11} \text{ Jm}^3 \text{ C}^{-2}$, $G_{12} = -2 \times 10^{-11} \text{ Jm}^3 \text{ C}^{-2}$, and $G_{44} = 2 \times 10^{-11} \text{ Jm}^3 \text{ C}^{-2}$.

In order to establish a better estimate of these coefficients, the GLD model is employed in the following to recalculate the polarization profiles of R71°, R109°, and R180°{110} FDWs at zero temperature using modified G coefficients, and the results are compared with first-principles ones. In order to facilitate the comparisons, these GLD model calculations have been performed on the identical geometries as in the first-principles calculations. That is, we impose periodic boundary conditions corresponding to the size of the first-principles supercells, impose the same twofold screw symmetry as was used there, and specify the strain state to be consistent with infinite domains.

C. Domain-wall width

In the case of a domain wall whose polarization profile can be fit to a hyperbolic tangent $p(x) = p_0 \tanh(x/\xi)$, a common definition of the width is $w = 2\xi$. However, some of the domain walls to be studied here have unusual polarization profiles that do not resemble a single hyperbolic tangent at all. To accommodate such cases, we define w as the width of the region within which $|p(x)|/p_0 < \tanh(1) = 0.762$. This definition has the advantages of being globally reasonably and of reducing to the conventional definition above when the FDW does resemble a hyperbolic tangent. We adopt this definition throughout the remainder of this work.

IV. RESULTS

BaTiO₃ has been studied extensively both experimentally and theoretically. Our first-principles computed values of 3.95 Å for the lattice constant and 89.93° for the rhombohedral angle can be compared with experimental values²¹ of 4.00 Å and 89.87°, respectively. Our results are consistent with the experience that the LDA typically gives slightly underestimated values for the unit-cell volume and ferroelectric distortion.²²

We have also computed the values of the dynamical charge tensors for cubic paraelectric BaTiO₃, to be used as an ingredient in the algorithm for computing polarization profiles as described in Sec. III A. The calculated values of Z^* for Ba, Ti, and O in BaTiO₃ are compared to the experimental values as well as ionic charges in Table I. The values of $Z_O \parallel$ and $Z_O \perp$ refer to the Z^* of the oxygen ion when it is displaced along the Ti-O direction or perpendicular to it, respectively.

TABLE I. The experimental and theoretical values of the dynamical effective charges of the Ba, Ti, and O atoms in BaTiO₃ (in units of the charge quantum e).

	Z_{Ba}	Z_{Ti}	$Z_{\text{O} \perp}$	$Z_{\text{O} \parallel}$
Nominal ionic	2	4	-2	-2
Z^* [Expt. (Ref. 23)]	2.9	6.7	-2.4	-4.8
Z^* (LDA)	2.75	7.18	-1.86	-5.65

A Berry-phase calculation of the polarization¹⁹ using the relaxed atomic positions in rhombohedral BaTiO₃ yields a value of 30 $\mu\text{C}/\text{cm}^2$. The polarization calculations using the atomic displacements and the theoretical Z^* values yield 31 $\mu\text{C}/\text{cm}^2$, which is slightly underestimated compared to the experimental value²¹ of 33.5 $\mu\text{C}/\text{cm}^2$ as expected. The GLD model, on the other hand, yields a value of 38 $\mu\text{C}/\text{cm}^2$.

In the following sections, we report the results of our supercell calculations for the R71°, R109°, and R180°{1 $\bar{1}$ 0} ferroelectric domain walls.

A. R71° domain wall

We have investigated the R71° FDW in rhombohedral BaTiO₃ by carrying out first-principles calculations on an 80-atom supercell made by stacking 10-atom rotated units as described in Sec. II. In this case, we only found an Ising FDW; perturbing this by adding symmetry-lowering components only led back to the Ising structure upon further relaxation. The polarization profile computed from the relaxed Ising structure using Eq. (2) is displayed in two ways in Figs. 5(a) and 5(b). The left panel, Fig. 5(a), shows the $P_r^{(l)}$ and $P_t^{(l)}$ values for each layer l , while Fig. 5(b) shows plots of $P_r^{(l)}$, $P_s^{(l)}$, and $P_t^{(l)}$ as a function of position s while scanning through a sequence of four domain walls (two entire supercells). As is clear from this figure, the P_t component remains zero everywhere in the supercell, which clearly indicates the Ising nature of this FDW. The P_r value reverses quite suddenly and attains a value very close to its saturation bulk value deep inside each domain, indicating a rather narrow FDW width. The P_s value is almost exactly constant; as we shall see, this is true of all FDWs in this study, consistent with the expectation that inhomogeneities in

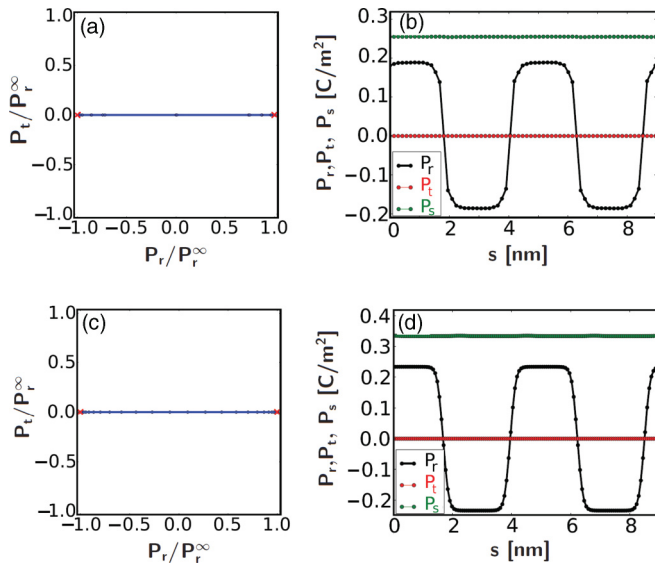


FIG. 5. (Color online) Polarization profiles of Ising R71° FDWs in rhombohedral BaTiO₃ as calculated using (a), (b) first-principles calculations, and (c), (d) the GLD model. Panels (a) and (c): parametric plots showing polarization values in the P_r - P_t plane. Crosses indicate local energy minima associated with homogeneous rhombohedral domains. Panels (b) and (d): polarization components as a function position s along the supercell direction (two supercells containing four FDWs are shown for clarity).

P_s would result in bound charge which in turn would involve an extra Coulomb energy cost.

The above results are in good qualitative agreement with those of the GLD model, but the GLD domain-wall width of 0.58 nm is almost twice that of the first-principles prediction of 0.33 nm. This suggests the need for a reduction of the zero-temperature values of the gradient terms in the GLD model to bring it into better agreement with the first-principles results. This reduction of the gradient terms will be even more important in the R180°{1 $\bar{1}$ 0} case, to be discussed in Sec. IV C. As explained there, we have chosen to reduce all three of the gradient coefficients in Eq. (5) by 40% in order to arrive at an improved GLD model.

The results computed for the R71° FDW using this modified GLD model are presented in Figs. 5(c) and 5(d) using the same plotting conventions as for the first-principles results in Figs. 5(a) and 5(b). The FDW width is now 0.37 nm. Furthermore, the GLD domain-wall energy is reduced from 5.0 to 3.2 mJ/m^2 , to be compared with the first-principles value of 3.8 mJ/m^2 . While these numerical values should be interpreted reservedly in view of the uncertainties in both theories, it is clear that the GLD theory is in better agreement with the first-principles theory after the reduction of the strength of the gradient term.

B. R109° domain wall

According to the GLD model calculations of Marton *et al.*,⁵ both Ising and Bloch solutions are possible for the R109° FDW in BaTiO₃. Our first-principles results confirm this picture. Starting first with the Ising case, Figs. 6(a) and 6(b) show the polarization profile for a 50-atom supercell in which the atomic positions have been relaxed from an initial configuration with two Ising-type R109° FDWs. The domain wall is again fairly narrow, though not quite as narrow as in the R71° case. The energy and width of this Ising R109° FDW are calculated from first principles to be 0.36 nm and 11.1 mJ/m^2 , respectively. The

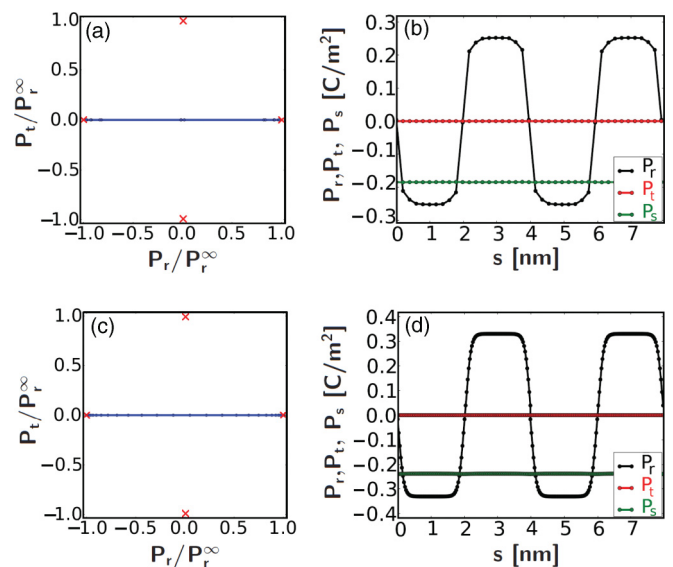


FIG. 6. (Color online) Polarization profiles for Ising R109° FDWs in BaTiO₃ using (a), (b) first-principles calculations and (c), (d) the GLD model. Details are as in Fig. 5.

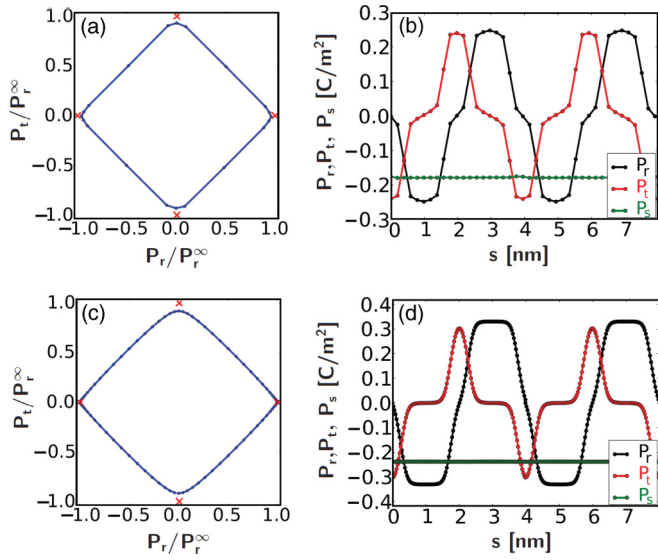


FIG. 7. (Color online) Polarization profiles for Bloch $R109^\circ$ FDWs in BaTiO_3 using (a), (b) first-principles calculations and (c), (d) the GLD model. Details are as in Fig. 5.

corresponding GLD results using the reduced gradient term, shown in Figs. 6(c) and 6(d), are clearly in good qualitative agreement.

When the atomic positions are relaxed from an appropriately distorted initial configuration, a Bloch-type solution for this wall is found. The first-principles polarization profiles computed for the Bloch-type $R109^\circ$ FDW in a 50-atom supercell are shown in Figs. 7(a) and 7(b). To a first approximation, this Bloch FDW can be regarded as a composition of two 71° FDWs in close proximity. In part for this reason, the Bloch-type FDW is clearly broader than the Ising one. However, the energies of the Bloch and Ising solutions are found to be almost identical, with the Ising one being only $\sim 2\%–3\%$ lower in energy. If we extrapolate to larger separations between FDWs, we might expect the Bloch energy to fall more than the Ising one because of the larger FDW width in the Bloch case. This suggests that both types of $R109^\circ$ FDWs have similar energies and that both might be found in rhombohedral BaTiO_3 crystals. The reason for the existence of both Ising and Bloch solutions for the $R109^\circ$ FDW is discussed in Sec. V. The modified GLD model again gives good qualitative and semiquantitative agreement with the first-principles results for the case of the Bloch $R109^\circ$ FDW, as shown in Figs. 7(c) and 7(d).

C. $R180^\circ\{1\bar{1}0\}$ domain wall

A major result of the GLD study of Marton *et al.*⁵ was the prediction that the lowest-energy FDW for the $R180^\circ\{1\bar{1}0\}$ case in BaTiO_3 is of Bloch type, with an energy lying 10% lower than that of its Ising counterpart. Verifying this result from first principles is computationally more challenging than studying the $R71^\circ$ or $R109^\circ$ FDWs. The $R180^\circ\{1\bar{1}0\}$ FDW has the biggest rotational angle and is hence the widest of the three investigated FDWs. Moreover, the Bloch-type FDWs are generally much broader than the Ising-type ones. Preliminary first-principles calculations showed that supercells smaller than 80 atoms are too small to accommodate two $R180^\circ$ FDWs;

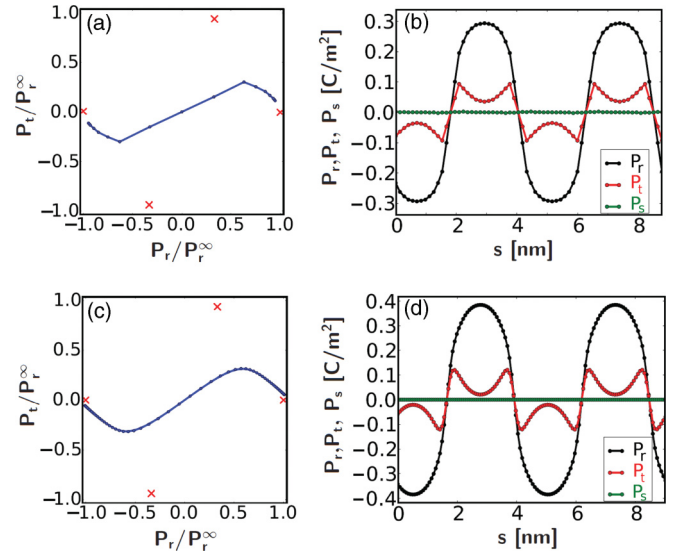


FIG. 8. (Color online) Polarization profiles for Ising $R180^\circ\{1\bar{1}0\}$ FDWs in BaTiO_3 using first-principles calculations. Details are as in Fig. 5.

initial 60-atom Bloch-wall supercells relaxed to unreasonable configurations. We have therefore carried out our calculations on an 80-atom supercell. While the polarization does not quite have room to reach its saturation value between neighboring FDWs, at least we obtain a stable solution that can reveal the Ising or Bloch nature of this FDW.

As mentioned in the last paragraph of Sec. II, it is possible to enforce an Ising-type geometry in the $R180^\circ\{1\bar{1}0\}$ case by imposing an initial inversion symmetry about an atom in the center of the FDW and preserving this symmetry during relaxation. When we apply our first-principles calculations including this symmetry constraint, we arrive at a configuration like that shown in Figs. 8(a) and 8(b), which is of Ising type in the sense that $P_r = P_t = 0$ in the center of the wall. However, P_s has substantial excursions away from zero, with the polarization path following an S-like curve in (P_r, P_t) space, as can be seen clearly in Fig. 8(a).

However, we find that if we do not impose this special symmetry, most initial conditions relax to the Bloch configuration shown in Figs. 9(a) and 9(b). Even if we start from an Ising-type configuration and break the symmetry only slightly, we find that the simulation will eventually relax to the Bloch configuration. It is clear from Figs. 9(a) and 9(b) that both P_r and P_t components are strongly nonzero, and the rotation of the polarization as one progresses through the domain wall, which is the characteristic feature of a Bloch-type wall, is clearly visible. It is also obvious that this Bloch FDW resembles an adjacent pair of 71° and 109° FDWs. We also find that this Bloch wall has a significantly lower energy than that of the Ising-type wall of Fig. 8, supporting the conclusion that the Bloch solution is the global minimum for the case of the $R180^\circ\{1\bar{1}0\}$ FDW.

We have also carried out corresponding simulations of the Ising-type and Bloch configurations of the $R180^\circ\{1\bar{1}0\}$ FDW using the GLD model. If this is done using the full strength of the gradient term under periodic boundary conditions, we find a stable Bloch solution only when the

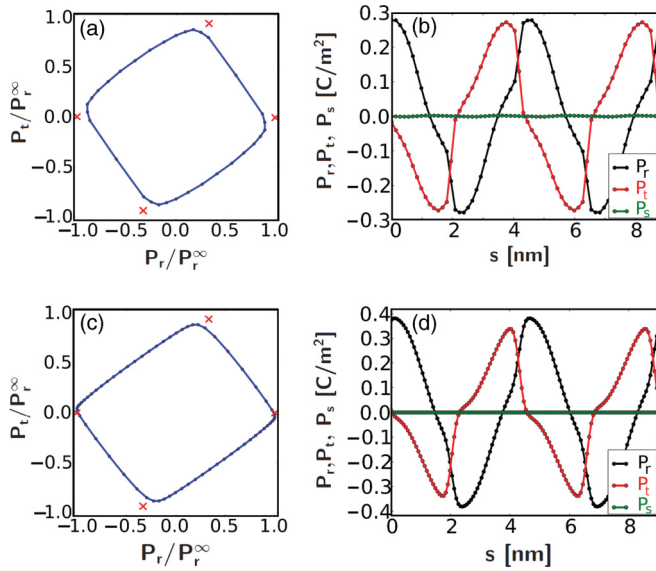


FIG. 9. (Color online) Polarization profiles for Bloch $R180^\circ\{1\bar{1}0\}$ FDWs in BaTiO₃ using (a), (b) first-principles calculations and (c), (d) the GLD model. Details are as in Fig. 5.

centers of the domain walls can be at least 3.4 nm apart. This is equivalent to using a supercell of 120 atoms in the first-principles calculations, and imposing the rhombohedral epitaxial strain does not change this result very much. On the other hand, we find that if the gradient term is reduced by about 40%, then stable solutions become possible under the same periodic boundary condition as in the 80-atom supercell. The polarization profiles calculated for the $R180^\circ\{1\bar{1}0\}$ FDWs using the GLD model with reduced gradient term, with the same domain-wall distance and elastic boundary conditions as in the first-principles calculations, are shown in Figs. 8(c) and 8(d) and 9(c) and 9(d) for the Ising-type and Bloch cases, respectively. The GLD results are clearly now in good qualitative agreement with the first-principles calculations.

The computed energies and widths of all of the FDWs are collected and presented in Table II. It is evident that the first-principles and GLD results are in broad agreement. As expected, the GLD model with reduced gradient term yields narrower walls and lower wall energies, yielding improved agreement for the Ising $R71^\circ$ and $R109^\circ$ cases, but somewhat overshooting for the Bloch $R109^\circ$ case.

TABLE II. Summary of computed energies and widths of $R71^\circ$, $R109^\circ$, and $R180^\circ\{1\bar{1}0\}$ FDWs in BaTiO₃. LDA indicates first-principles results; GLD and GLD-r refer to the Ginzburg-Landau-Devonshire model with original and reduced gradient terms, respectively.

	Wall width (nm)			Wall energy (mJ/m ²)		
	LDA	GLD	GLD-r	LDA	GLD	GLD-r
Ising $R71^\circ$	0.33	0.58	0.37	3.8	5.0	3.2
Ising $R109^\circ$	0.36	0.54	0.34	11.1	10.6	6.8
Bloch $R109^\circ$	1.01	1.10	0.72	11.2	10.2	6.2
Ising $R180^\circ$	0.51		0.83	26.6		27.2
Bloch $R180^\circ$	1.38		1.40	24.0		27.6

For the $R180^\circ$ FDWs, the values given in Table II ought not be taken too seriously because the repeat distance of the supercell is rather short compared to the FDW width. In fact, we did not succeed in finding stable FDW solutions with the original GLD model. The present 80-atom supercell is large enough to give stable solutions in both the LDA and reduced-GLD calculations, but their properties are undoubtedly not yet converged with supercell size. The FDW energy can be expected to fall with supercell size, so the energies in Table II should be taken as upper bounds. The ‘‘crowding’’ of the Bloch $R180^\circ$ walls appears to be more serious than for the Ising ones, which can explain why the reduced GLD model predicts a slightly higher energy for the Bloch compared to the Ising FDW. When the GLD calculations are repeated for larger FDW separations, they clearly predict that the Bloch configuration is lower in energy.⁵ The first-principles calculations already predict the Bloch wall to be lower in energy for the 80-atom supercell, and this trend would only be strengthened if we could afford to repeat the calculations at increasingly larger FDW separations such that well-developed rhombohedral domains could form between domains.

V. DISCUSSION

Among the three investigated FDWs, the polarization vector rotates by the smallest angle in the $R71^\circ$ FDW, and by the biggest angle in the $R180^\circ\{1\bar{1}0\}$ FDW, so it is not surprising that the former has the smallest energy and the latter the biggest, as summarized in Table II. We can also propose a simple explanation for the fact that the first-principles calculations and the GLD model results predict an Ising nature for the $R71^\circ$ FDW, a Bloch nature for the $R180^\circ\{1\bar{1}0\}$ FDW, and a very small energy difference between Ising and Bloch solutions for the $R109^\circ$ FDW. The path the polarization vector would take in rotating from one side of the wall to the other in a Bloch-type solution is shown for each of these FDWs in Fig. 10. In a hypothetical Bloch $R71^\circ$ FDW, the polarization vector would pass close to the center of one of the adjacent faces, which corresponds to a tetragonal polarization state and is not energetically favorable in the rhombohedral phase.

On the other hand, the Bloch 109° FDW can be considered as a combination of two $R71^\circ$ FDWs. As can be seen from Table II, the total energy of two Ising $R71^\circ$ FDWs is rather close to the energy of one Ising 109° FDW, from both the LDA and GLD calculations. By way of a caveat, we point

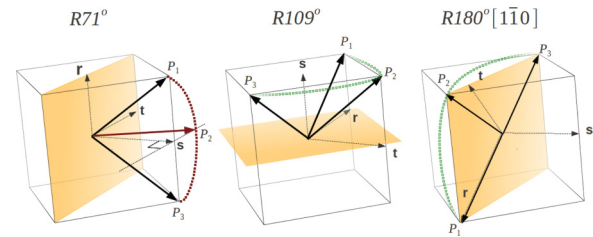


FIG. 10. (Color online) The path swept by the tip of the polarization vector while rotating from \mathbf{P}_1 to \mathbf{P}_3 when crossing through hypothetical Bloch-type FDWs for the $R71^\circ$, $R109^\circ$, and $R180^\circ\{1\bar{1}0\}$ geometries. For the $R71^\circ$ case, the path (which rotates in a plane parallel to the FDW) is shown in red to indicate that it is unfavorable.

out that such a comparison may be overly simplistic because the Ising walls comprising the Bloch 109° FDW experience a foreign strain environment and do not conform to the plane of mechanical compatibility of a true $R71^\circ$ FDW. Nevertheless, the comparison does hint that we should not be surprised to find the Ising and Bloch configurations to be competitive here. Finally, for the Bloch $180^\circ\{1\bar{1}0\}$ FDW, which can be regarded as one $R71^\circ$ FDW plus one $R109^\circ$ FDW, the LDA calculations indicate that the sum of the energies of these two walls is much lower than that of a single Ising 180° FDW. The above caveat has perhaps even more force here, but again we can roughly understand in these terms why the $R180^\circ\{1\bar{1}0\}$ FDW can only adopt a Bloch form.

VI. SUMMARY

In conclusion, we have calculated the domain-wall widths, energies, and polarization profiles for Ising and Bloch ferroelectric domain walls in the zero-temperature rhombohedral phase of BaTiO_3 using both first-principles and Ginzburg-Landau-Devonshire methods. The first-principles results confirm the expectation that 180° domain walls are of Bloch type, adopting a configuration resembling a pair of 109° and 71° walls in close proximity. For the case of the 109° wall, Ising and Bloch configurations are competitive. The Ginzburg-Landau-

Devonshire results are brought into improved agreement with the first-principles calculations if the coefficient of the gradient term is reduced by about 40%. In view of the uncertainties in the original extraction procedure for the coefficients, it is not surprising that these parameters can be improved; indeed, it is encouraging that even the original parameters gave qualitatively sound results.

While we have not extended our work to other rhombohedral ferroelectrics such as KNbO_3 , we expect that these may show a similar pattern of behavior. When instabilities other than ferroelectric ones are also present, the domain-wall behavior can become more complicated, as for example with the octahedral rotations and magnetic ordering that play a role in BiFeO_3 .¹⁰ However, we hope that this work will serve as a useful benchmark for domain walls in rhombohedral ferroelectrics generally, and will lead to an improved understanding of ferroelectric domain dynamics and switching in these systems.

ACKNOWLEDGMENT

This work was supported by ONR Grant No. N00014-05-1-0054 and by Project No. GACR P204/10/0616 of the Czech Science Foundation.

*mtaheri@physics.rutgers.edu

¹Y. L. Wang *et al.*, *J. Appl. Phys.* **110**, 014101 (2011).

²B. Meyer and D. Vanderbilt, *Phys. Rev. B* **65**, 104111 (2002).

³D. Lee, R. K. Behera, P. Wu, H. Xu, Y. L. Li, S. B. Sinnott, S. R. Phillpot, L. Q. Chen, and V. Gopalan, *Phys. Rev. B* **80**, 060102(R) (2009).

⁴R. K. Behera *et al.*, *J. Phys.: Condens. Matter* **23**, 175902 (2011).

⁵P. Marton, I. Rychetsky, and J. Hlinka, *Phys. Rev. B* **81**, 144125 (2010).

⁶H. D. Megaw, *Nature (London)* **155**, 484 (1945).

⁷A. Von Hippel, R. G. Breckenridge, F. G. Chesley, and L. Tisza, *Ind. Eng. Chem.* **38**, 1097 (1946).

⁸B. Wul and I. M. Goldman, C. R. (Dokl.) Acad. Sci. URSS **51**, 21 (1946).

⁹J. Padilla, W. Zhong, and D. Vanderbilt, *Phys. Rev. B* **53**, R5969 (1996).

¹⁰A. Lubk, S. Gemming, and N. A. Spaldin, *Phys. Rev. B* **80**, 104110 (2009).

¹¹Hohenberg and W. Kohn, *Phys. Rev.* **136**, B864 (1964); W. Kohn and L. J. Sham, *ibid.* **140**, 1133 (1965).

¹²J. P. Perdew and A. Zunger, *Phys. Rev. B* **23**, 5048 (1981).

¹³D. Vanderbilt, *Phys. Rev. B* **41**, 7892 (1990).

¹⁴P. E. Blöchl, *Phys. Rev. B* **50**, 17953 (1994).

¹⁵C. G. Broyden, *Notices Am. Math. Soc.* **16**, 670 (1969); R. Fletcher, *Comput. J.* **13**, 317 (1970); D. Goldfarb, *Mathematics of Computation* **24**, 23 (1970); D. F. Shanno, *ibid.* **24**, 647 (1970).

¹⁶H. J. Monkhorst and J. D. Pack, *Phys. Rev. B* **13**, 5188 (1976).

¹⁷W. Zhong, R. D. King-Smith, and D. Vanderbilt, *Phys. Rev. Lett.* **72**, 3618 (1994).

¹⁸The dynamical effective charge tensors in the rhombohedral phase are anisotropic and depend on the rhombohedral axis. We thus use the cubic tensors instead; we judge this to be a reasonable approximation within the intended accuracy of our calculations.

¹⁹D. Vanderbilt and R. D. King-Smith, *Phys. Rev. B* **48**, 4442 (1993).

²⁰J. Hlinka and P. Marton, *Phys. Rev. B* **74**, 104104 (2006).

²¹W. Hewat, *Ferroelectrics* **6**, 215 (1974).

²²K. Rabe and Ph. Ghosez, *Physics of Ferroelectrics: a Modern Perspective*, edited by K. M. Rabe, C. H. Ahn, and J.-M. Triscone (Springer-Verlag, Berlin, 2007), pp. 117–174.

²³J. D. Axe, *Phys. Rev.* **157**, 429 (1967).